European Polymer Journal 219 (2024) 113397

Contents lists available at ScienceDirect

European Polymer Journal

journal homepage: www.elsevier.com/locate/europolj

Boosting *m*-aramids performance with *p*-oriented aromatic amide side chains

Álvaro Miguel-Ortega [a,b], Sául Vallejos [a], José Miguel García [a], Miriam Trigo-López [a,*]

[a] Departamento de Química, Facultad de Ciencias, Universidad de Burgos, Plaza de Misael Bañuelos s/n, 09001 Burgos, Spain
[b] Facultad de Ciencias, Universidad Autónoma de Madrid, Calle Francisco Tomás y Valiente 7, Fuencarral-El Pardo, 28049 Madrid, Spain

ARTICLE INFO

Keywords:
Mechanical performance
thermal properties
hydrogen bonding
high performance
side chain
application in hydrogen environments.

ABSTRACT

This study aimed to enhance the mechanical properties of *m*-aramids by incorporating varying percentages of *p*-aramid side chains through copolymerization while ensuring solubility for practical applications. The mechanical performance of the resulting copolymers was compared with the commercial *m*-aramid, MPIA (poly(*m*-phenylene terephthalamide)). Notably, even with a 20% incorporation of *p*-aramid side chains, there was a substantial increase of 48% in Young's modulus and 7% in tensile strength compared to MPIA. Additionally, the nitro group capping the *p*-aramid side chains demonstrated significant efficacy in enhancing the mechanical performance of the materials upon exposure to hydrogen. Specifically, there was an increase of more than 11% in Young's modulus upon initial contact with hydrogen. This finding suggests potential applications in protective coatings for stainless steel used in high-pressure hydrogen storage environments. In such applications, exposure to hydrogen can accelerate embrittlement and limit operational lifespan, and coating with these materials can mitigate embrittlement and improve operational lifespan.

1. Introduction

Aramids or aromatic polyamides are high-performance polymeric materials known for their properties, keeping their strength at elevated temperatures and resisting permanent deformation. The most well-known aromatic polyamides are poly(*p*-phenylene terephthalamide), PPTA, and poly(*m*-phenylene isophthalamide) or MPIA, which are also commercial. Their toughness exceeds that of steel, glass fibre, and nylon, and they exhibit durability even when subjected to extreme tension and bending, showcasing their remarkable versatility. Additionally, their high (electro)chemical stability, stemming from their resonance structure, makes them suitable for applications requiring insulation and chemical resistance. These properties arise from their rigid rod-like backbone of aromatic rings and amide groups [1,2]. Aromatic groups provide π-π staking interactions, while amide groups enhance hydrogen bonding between polymer chains, significantly boosting internal cohesion in the solid state. The properties of PPTA and MPIA differ due to their backbone structures' all-*para* and all-*meta* orientation, respectively. PPTA's all-para orientation contributes to its exceptional strength, which is up to five times stronger than steel by weight, with high wear resistance, a lightweight nature, and good chemical resistance. This makes it a popular choice for bulletproof vests, reinforced tires, ropes, and high-strength applications. Conversely, MPIA's all-*meta* orientation leads to poorer tensile properties than PPTA due to the lower chain packaging. However, MPIA is valued for its thermal resistance, tensile strength, flexibility, and ability to maintain mechanical properties at high temperatures. Notably, its thermal stability surpasses that of PPTA, demonstrating excellent resistance to high temperatures without melting or burning easily, making it highly fire-resistant. MPIA finds widespread use in critical applications requiring heat and flame resistance, including firefighter and pilot suits, and within the automotive industry. Despite these merits, aramid polymers exhibit infusibility, and their low solubility in usual organic solvents complicates their production and processing, limiting their applications. This is especially true for PPTA, which only dissolves in concentrated sulfuric acid, while MPIA dissolves in polar aprotic solvents [3].

To summarize, while MPIA and PPTA share similarities in chemical structure and thermal properties, they differ significantly in mechanical strength and rigidity. PPTA is notably stronger and more rigid, whereas MPIA is prized for its flexibility and superior fire resistance. But, if we were able to synthesize a polymer with a chemical structure that bridges the characteristics of PPTA and MPIA, what properties might it exhibit?

* Corresponding author.
E-mail address: mtrigo@ubu.es (M. Trigo-López).

https://doi.org/10.1016/j.eurpolymj.2024.113397
Received 2 May 2024; Received in revised form 30 July 2024; Accepted 19 August 2024
Available online 19 August 2024

One of the main objectives in aramid's research is the improvement of the mechanical performance of MPIA while maintaining its thermal performance and keeping or improving its solubility. In this sense, molecular design involving the precise tailoring of polymeric structure is crucial for endowing aramids with unique physical and chemical properties and enhanced capabilities, facilitating manufacturing and expanding their applications. Different strategies have been followed for this purpose, including the design of aramids with additional physical interchain interactions or even crosslinking [4]. Hence, alternatives to leveraging supramolecular forces like the ones present in *p*-aramids (directional hydrogen bonds and aromatic stacking), some kind of "self-reinforcement", present expansive opportunities for customizing and fine-tuning the physical and chemical properties of polymers [5]. The use of aramid-like side chains in polymers to provide additional hydrogen interactions has only been described to improve the thermal performance of polystyrene grafting poly(*p*-benzaime) side chains [6], to prepare comb-like poly(norbornene)s with an improvement of their properties [7], and for surface-initiated aramid polymer brushes grown from silicon wafers and silica particle [8]. However, the exploration of aramids containing aramid rod-like side chains has never been addressed to our knowledge.

Accordingly, and aiming to improve the mechanical performance of MPIA through a self-reinforcing approach by preparing a polymer with a chemical structure bridging MPIA and PPTA, we have developed *m*-oriented brush aramids containing *p*-oriented aromatic amide groups in the shape of side rod-like chains. In order to establish correlations between the structure and properties of polymers to develop aramids with improved properties, we designed a diacid chloride monomer containing an aramid rod-like structure (Figure 1). The monomer was copolymerized in different proportions (1-50%) with isophthaloyl dichloride and *m*-phenylene diamine. Four different random copolymers were obtained, and we investigated the impact of rod-like aramid side chains in *m*-aramids, as well as the influence of their concentration within the polymer on aramids' mechanical and thermal properties. Our research provides a comprehensive understanding of the interplay between structure and properties, thereby paving the way for innovative approaches in the tailored design of aramids. As a progressive approach, we engineered these aramids to terminate their side chains with a nitro group. We have demonstrated that this nitro group can be reduced in the solid state in the presence of hydrogen under pressure, resulting in improved mechanical properties in the copolymer, as graphically depicted in Figure 1. This advancement significantly expands the potential applications of these materials beyond protective equipment or separation membranes, particularly in fields associated with high-performance coatings on steel for hydrogen storage and transport, to advance in the field of hydrogen economy and the reduction of fuel dependence.

2. Materials and Methods

2.1. Materials

All the materials utilized in this work are commercially accessible and were used without any alterations unless otherwise specified: *N,N*-dimethylacetamide (DMA, VWR Chemicals, >99%), 5-aminoisophthalic acid (Sigma Aldrich, 94%), 4-nitrobenzoyl chloride (Thermo Fischer, 98%), ethyl acetate (VWR Chemicals, 99,9%), *N,N*-dimethylformamide (DMF, Merck, >99%), palladium on activated charcoal (Pd/C, Merck, 10%Pd), and sodium nitrite ($NaNO_2$, Panreac, >98%). Lithium chloride (LiCl, VWR Chemicals, ≥ 99%) was dried inside a furnace at 400 °C for 12 h before use. *N*-Methyl-2-pyrrolidone (NMP, VWR Chemicals, >99.5%) was subjected to two rounds of vacuum distillation using phosphorus pentoxide (P_2O_5, Alfa Aesar, 98%) and subsequently stored alongside 4 Å molecular sieves. Triphenylphosphite (TPP, TCI, ≥ 97%) was distilled twice using high-vacuum and stored in 4 Å molecular sieves. Pyridine (Thermo Scientific, 99,5%) was dried under reflux over NaOH (VWR Chemicals, 99%) for 24 h, distilled twice and kept stored in 4 Å molecular sieves. *m*-Phenylenediamine (MPD, Sigma-Aldrich, 99%) underwent purification via dual vacuum sublimation and was then stored under nitrogen. Isophthalic acid (TCI, >99%) was crystallized twice from water.

2.2. Methods

A Bruker Avance III HD spectrometer running at 300 MHz and 75 MHz was employed to acquire the ^{1}H and ^{13}C NMR spectra, respectively, using deuterated dimethylsulphoxide (DMSO-d_6) as the solvent.

Infrared spectra (FTIR) of the intermediates, monomers, and polymers were acquired after vacuum drying them and using an FT/IR-4200 Jasco spectrometer coupled with an ATR-PRO410-S accessory.

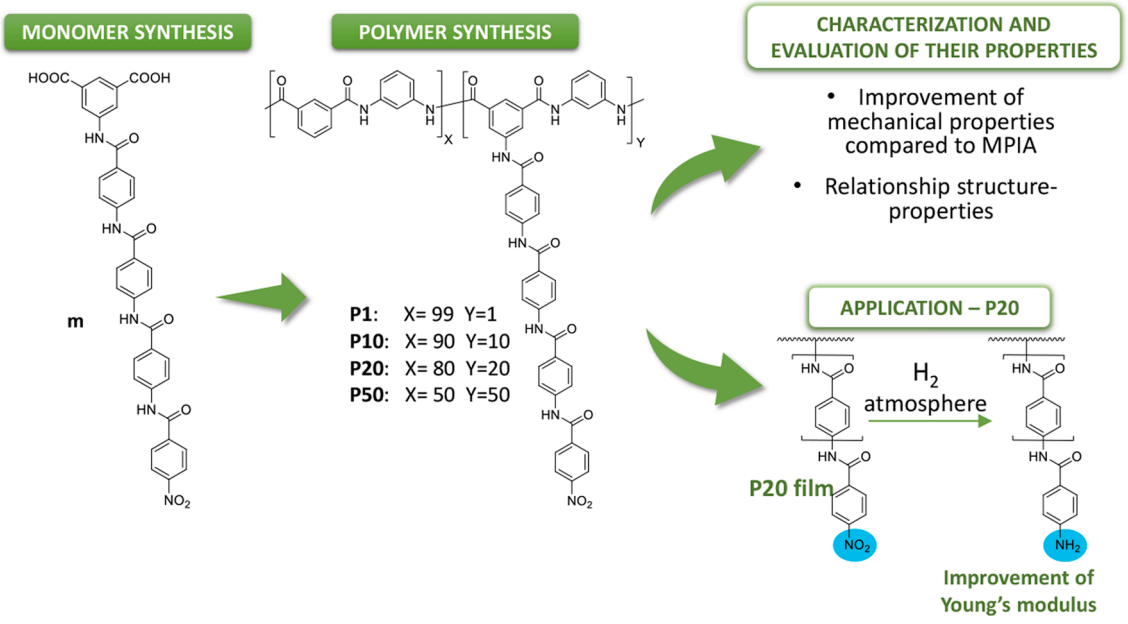

Figure 1. Work objectives and methodology.

The intermediates and monomer mass spectrometry (MS) was acquired with an Agilent 6545 Q-TOF coupled with an electrospray ionization source (Agilent Jetstream Technology AJT-ESI).

The thermal performance of the polymers was analyzed in terms of thermogravimetric analysis (TGA) using samples of about 5 mg under nitrogen and air atmospheres on a TGA Q50 (TA Instruments) analyzer at 10 °C/min. The limiting oxygen index (LOI) was calculated from the char yield (CR, weight% at 800 °C) taken from the measurement under nitrogen and using the Van Krevelen equation (LOI = 17.5 + 0.4 CR) [9]. Also, the thermal performance was analyzed using differential scanning calorimetry (DSC). The tests were performed to verify the thermal transitions of the copolymers using a DSC Q200 (TA Instruments) with a nitrogen flow of 50 mL/min and using 15 mg polymer samples. The DSC experiments were executed as follows: first, the temperature was equilibrated at -80 °C/min; then, a ramp up to 300 °C at a speed of 10 °C/min was performed to delete the thermal history of the material. After that, the sample is cooled down to -80 °C at a speed of 10 °C/min. Lastly, the sample is heated to 300 °C and cooled at -80 °C at a speed of 10 °C/min.

The solubility of the materials was evaluated by combining 10 mg of the copolymer with 1 mL of solvent. The mixture is stirred at 20 °C for 24 hours. A homogeneous solution indicates the polymer's solubility. If not soluble, the mixture was heated to reflux for two hours to assess solubility under elevated temperature conditions. The polymer is deemed soluble upon heating if a uniform clear solution is achieved. Alternatively, the polymer is considered insoluble if no uniform clear solution is attained.

The inherent viscosity η_{inh}, of the copolymers was assessed using a viscometer (Canon-Fenske) with a concentration of the polymer of 0.5 g/dL in DMA containing 5% of LiCl (solvent) and at 25 °C. The intrinsic viscosity [η], was calculated by measuring the inherent viscosity at various concentrations of the polymer (0.05, 0.1, 0.3, 0.5 g/dL) using DMA (5% LiCl) as the solvent and extrapolating to zero concentration. The viscometric equation (Mark-Houwink-Sakurada (MKS) equation) $[\eta] = \kappa M_{\omega}^{\alpha}$ (for MPIA $\kappa = 0.00013$ dL/g and $\alpha = 0.84$)[10] was used to estimate the average molecular mass (M_w).

Water uptake experiments were carried out gravimetrically with vacuum-dried fibrous swollen polymers (around 20-25 mg samples dried overnight at 80 °C under phosphorous pentoxide). The polymers are placed in a closed container in the presence of a concentrated solution of $NaNO_2$ at 20 °C to provide a 65% relative humidity environment. The polymer samples are weighed regularly until no variation in the sample's mass is observed. The calculation of water molecules per structural unit considers the structural unit's weight and water absorption. Regarding copolymers, the calculation of a hypothetical structural unit involves taking into account the weight ratio of the two structural units of the copolymers.

The aramid film's mechanical behaviour was measured using a EZ Test Compact Table-Top Universal tester machine (Shimadzu) on 5 × 30 mm strips. The tests were completed using a 5 mm/min extension rate and 9.44 mm gauge length. At least five strips of every film were tested, and the results were then averaged, excluding the highest and lowest values for each film.

The films X-Ray diffraction spectra were attained using a D8 Discover DaVinci diffractometer (Bruker), coupled with a LINXEYE XE high-resolution energy-dispersive detector. The 2θ angle swept was measured from 2.5 to 90°, with a step size of 0.05° and 0.5 seconds per step.

The Young's moduli were locally measured using AFM microscopy (Cipher ES Environmental AFM, Oxford Instruments), using the AM–FM viscoelastic mapping mode as described elsewhere [11]. The microscope was equipped with a 160AC-NA tip (Opus, Mikromasch). The acquisition and Young's modulus calculation software used was Asylum AR 16.23.224 (Oxford Instruments, Asylum Research, Wiesbaden, Germany) and the images were processed using the Gwyddion 2.63 software. The samples were deposited in AFM steel Ø15mm discs (Ted Pella,). Images were recorded with 512X512 lines, at 10x10 μm, 5x5 μm, 2,5x2,5 μm and 1.25x1.25 μm, in which the Young's modulus was calculated for each of the images.

2.3. Synthesis of copolymers P1, P10, P20 and P50.

Synthesis of copolymer P1: First, monomer **m** was synthesized through a series of high-yield, well-established organic synthetic reactions, involving subsequent condensation and hydrogenation steps, initiated from 4-nitrobenzoyl chloride and 5-aminoisophthalic acid, as outlined in the Supplementary Information (SI), Section S1. The copolymer was prepared using a three-necked round flask with a stirrer (mechanical stirring) filled with a nitrogen atmosphere. NMP (40,9 mL) was added to the flask. The system was heated to 110 °C and then *m*-phenylene diamine (2.210 g, 0.0205 mol), pyridine (12.27 mL, 0.1523 mol), and TPP (11.83 mL, 0.0450 mol) was added and stirred until full solution. 0.141 g (2.045 x10^{-4} mol) of monomer **m** and 3.360 g (0.0202mol) of isophthalic acid are added to the flask. The system is stirred for 4 hours, cooled down to about 20-25 °C and poured into methanol, obtaining a swollen white precipitate that was filtered and washed with methanol, water and acetone (a quantitative yield is obtained).

Synthesis of copolymer P10, P20 and P50: The synthesis procedure is the same as for **P1**, but the loading proportions of the monomers are different. For **P10,** 4.12 x 10^{-3} mol of *m*-phenylenediamine, 0.03 mol of pyridine, 8.98 x 10^{-3} mol of TPP, 0.412 x 10^{-3} mol of **m** and 3.71 x 10^{-3} mol of isophthalic acid were added. For **P20,** 0.0146 mol of *m*-phenylenediamine, 0.11 mol of pyridine, 0.02 mol of TPP, 17.46 x 10^{-3} mol of **m** and 0.007 mol of isophthalic acid were added. For **P50,** 0.01 mol of *m*-phenylenediamine, 10 mmol of pyridine, 0.022 mol of TPP, 5 mmol of **m** and 5 mmol of isophthalic acid were added.

2.4. Preparation of polymer films

Films of the polymers were obtained using the general solution-evaporation (casting) technique using DMA (5 mL) as the solvent and 7% by polymer mass (0.35 g). The solution was placed on a glass surface in the interior of a ventilated oven at 80 °C for 24 h to eliminate the solvent. After that, the polymer films were stirred with water at 60 °C to wash them and remove any solvent residues.

2.5. Proof of concept

Two different films were prepared to evaluate the behaviour of the copolymer **P20** under pressured H_2. First, a stock solution of 1.4 g of **P20** in 10 mL of DMA (14 wt%) was prepared. Then 3 mL of the stock solution was placed on a glass, the DMA was removed at 60 °C, and a film was obtained. Another portion of 3 mL was placed into a vial and 8.4 mg of 10% Pd/C catalyst was added (2 wt%) and stirred. Then, the mixture was placed on a glass surface and the DMA was eliminated at 60 °C. Both films were let dry overnight, and then washed with water.

Once the films were obtained, they were placed in a glass flask, to fill with H_2. To homogenize the atmosphere inside the flask, it was filled with H_2 at 30 psi for 5 minutes and then the flask was emptied. This process was repeated three times. After that, the flask was filled with H_2 at 70 psi of pressure and let overnight under that pressure. The next day, the films were removed from the flask and characterized.

3. Results and discussion

3.1. Monomer and copolymers synthesis

To prepare the copolymers, we first synthesized a monomer containing *p*-oriented amide groups in the pendant structure according to the procedures described in the (SI), Section S1.. The synthesis and characterization of intermediates **1** and **2** was previously described [12],

and the rest of the intermediates were synthesized following a straightforward method with common organic synthesis reactions and in high yields and high purity, as corroborated using NMR spectra. Moreover, the reactants used for the synthesis of the monomer were commercial and inexpensive. The structure of the intermediates and monomer was assessed by FTIR, mass spectrometry and both ^{1}H and ^{13}C NMR (see Figures S1 to S8 in SI, Section S1). We initially wanted to synthesize a monomer with more *p*-aromatic moieties to highlight the effect of the *p*-aramid side chain structure on the polymer properties. However, as the length of the monomer increased, its solubility decreased due to the *p*-aromatic nature, making it more insoluble in the reaction media.

The copolymers were prepared following the Yamazaki-Higashi high-temperature condensation procedure, using *m*-phenylene diamine and isophthalic acid as comonomers. The structure of the copolymers is shown in Figure 2, and was confirmed by ^{1}H and ^{13}C NMR spectra, which agree with the copolyamides chemical structure and the monomer loading percentages (see Figures S9 to S12, SI, Section S2). Additionally, the inherent viscosities of the copolymers were measured to estimate the molecular mass of the polymers (Table 1) using the MKS equation for poly(*m*-phenylene isophthalamide) (MPIA), demonstrating a high degree of polycondensation, and indicating their capability for industrial processing. Initially, we intended to synthesize copolymers from this monomer using the low-temperature procedure commonly employed in the industrial synthesis of *m*-aramids, where diacid chlorides are used instead of diacids. However, we encountered difficulties with the preparation of **P20** and **P50** using this method. The high loading percentage of monomer **m** under these polymerization conditions led to monomer insolubility due to its *p*-aramid nature, making it impossible to prepare the aramids in this manner. Therefore, we decided to prepare all the copolymers using the high-temperature procedure to ensure uniformity.

The copolymers prepared from this monomer contain amides, which provide additional interchain and interside chain interactions through hydrogen bonding. We prepared four different copolymers containing different proportions of the amide-containing monomer, to evaluate the impact of the pendant chain on the thermal and mechanical performances of the resulting copolymers (Figure 2). We also prepared a commercial *m*-aramid (MPIA) following the procedure described [13] to compare its properties with the new materials.

3.2. Polymers properties

3.2.1. Water uptake and solubility

Regarding the solubility of the copolymers, two facts should be considered. Firstly, one would expect the new copolymers to show improved solubility compared to commercial *m*-aramid due to the bulky side group that impairs the hydrogen bond formation between two adjacent polymer main chains, reducing polymer packaging efficiency and crystallinity. Secondly, the amides located in the side chain of the copolymers, are expected to provide additional hydrogen bond interactions with other side chains and with another polymer main chain, which would result in poorer solubility. The solubilities of the polymers are described in Table 1. As anticipated, all the copolymers proved to be soluble solely in polar aprotic solvents under the testing conditions, in addition to acids, such as sulfuric acid. These conditions are typically employed for assessing the solubility of aramids, and seemingly, no distinctions were discernible among the tested polymers. However, subtle variations were noted during the testing process, and for copolymer **P50,** it was impossible to prepare a solution of concentration higher than 4% (mass/volume) in DMA, impairing the preparation of films to evaluate some of the properties of this copolymer. Also, as the monomer intermediates were prepared, we observed that with each increase in the length of the intermediate, it became more insoluble, consistent with the expected behaviour of a *p*-aramid rod-like structure. This led us to decide against further enlarging the monomer.

The water uptake of the polymers was also tested (Table 1). A high amount of water uptake can be beneficial for certain applications, such as membranes for water desalination, and undesirable for others, since water weakens amide-amide interactions, resulting in poorer mechanical and thermal performances. The amide link of the aramids is highly polar, tending to absorb environmental water. Although the water uptake is higher for the synthesized aramids compared to the commercial one (in weight perecent), this percentage only increases slightly. Considering the number of water molecules per structural unit (calculated as the average molecular weight of the two structural units and their proportion), a trend can be observed, showing an increase with a higher percentage of *p*-aramid side chain. However, considering the water uptake per amide group, it was calculated to be 0.01 water molecule per amide group for all polymers. Explaining the water uptake results is complex, as several factors influence it. The presence of polar amide groups should theoretically increase water uptake, while hydrogen bonding between the main and side chains of the polymers can hinder water uptake. Also, the availability of the amide groups influences the final water uptake. Unfortunately, these effects cannot be studied in isolation since they depend on each other.

3.2.2. Infrared spectroscopy

Infrared spectroscopy of the films was studied to confirm the copolymer's structure and elucidate hydrogen bond interactions within

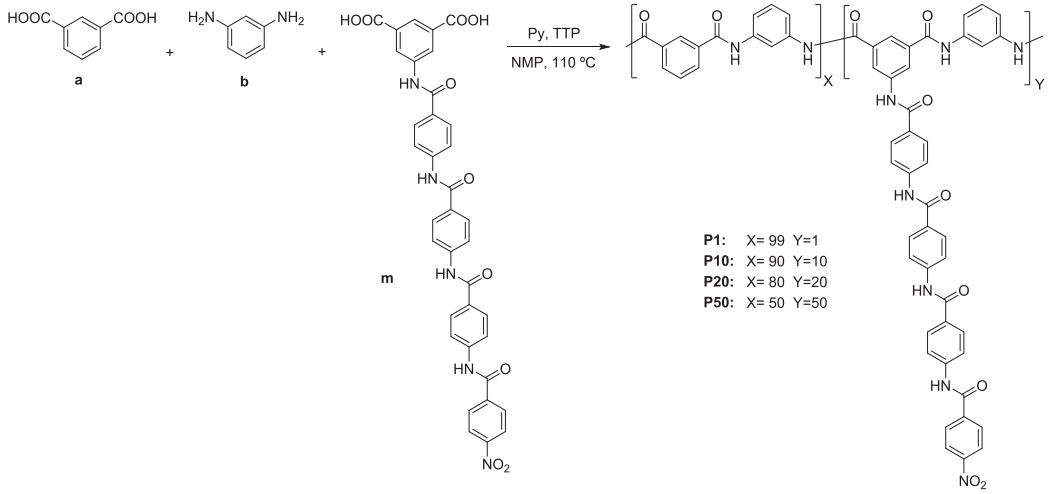

Figure 2. Polymers synthesis and composition

Table 1
Inherent viscosity, intrinsic viscosity, molecular mass, water uptake and solubility of copolymers P1, P10, P20, P50 and the reference *m*-aramid.

Polymer	η_{inh} [a] (dL/g)	$[\eta]$ [b] (dL/g)	Mw [c] (kDa)	Water Uptake [d]		Solubility [e]				
				Mass (%)	Water Molecules per Structural Unit [f]	DMA	DMF	DMSO	NMP	CH_2Cl_2, $CHCl_3$, EtOH, THF, Acetone
P1	1.04	1.67	78	6.3	0.87	++	++	++	++	−
P10	1.46	3.06	160	7.6	1.24	++	++	++	++	−
P20	1.09	2.26	111	6.6	1.26	++	++	++	++	−
P50	2.78	3.45	184	6.8	1.89	++	++	++	++	−
MPIA[g]	1.04	1.06	69	5.2	1.20	++	++	++	++	−

[a] 0.5 g/dL solution in DMA (5% LiCl). [b] Calculated using 0.5, 0.3, 0.1 and 0.05 g/dL solution in (5% LiCl). [c] From $[\eta]$ and the MKS equation and viscometric parameters of MPIA ($\kappa = 0.00013$ dL/g; $\alpha = 0.84$) [10]. [d] Relative humidity = 65%, Temperature = 20 °C. [e] 10 mg of polymer/1 mL of solvent; ++ = soluble at 20 °C; + = soluble on heating; +− = partially soluble; − = insoluble. [f] Hypothetical structural unit in copolymers, estimated using the mass and feed ratio of the aramid. [g] MPIA synthesized in the laboratory.

the copolymer. The full FTIR spectra of the polymers are depicted in Figure 3a). Aramids' main chain interacts with other polymer chains through amide groups, forming hydrogen bonds, which are responsible for aramids' properties. Hydrogen bonds can be distinguished using infrared spectroscopy due to their characteristic effects on the vibrational modes of the molecules involved. However, some free amide groups in aramids do not form hydrogen bonds, in agreement with the FTIR spectrum of **MPIA** [14]. In the lack of hydrogen bonding, the stretching vibration of the N-H bond shows up at around 3300-3500 cm^{-1} in the infrared spectrum. However, when hydrogen bonding occurs between adjacent amide groups, it affects the vibrational frequencies of the N-H bond, resulting in the shift of the N-H stretching vibration to lower wavenumbers, appearing at around 3100-3300 cm^{-1}. This fact can be observed in the synthesized copolymers, as the free N-H stretching band disappears as the amount of aramid side chains increases from **P1** to **P50**, attributable to the formation of hydrogen bonds between the N-H and the C=O groups in the copolymers (Figure 3b). Amide I band is also sensitive to the hydrogen bonds formation. The C=O stretching band observed at 1647 cm^{-1} for **MPIA**, is a combination of different C=O amide bands in the synthesized copolymers, reflecting the diverse chemical environments of different amide groups within the copolymer structure, both in the main chain and the side chain. Consequently, the impact of hydrogen bonding on this band is not easily discernible in the spectra, with only subtle changes in intensity and width becoming evident as the number of side chains increases. The deconvolution of this band (Figure 3d) revealed the presence of two distinct bands in the synthesized copolymers. For **P1**, two bands can be observed at 1666 cm^{-1} and 1648 cm^{-1}. This is attributed to the fact that when hydrogen bonding occurs between the carbonyl oxygen (C=O) and the hydrogen atom of a neighbouring amide group, it can lead to changes in the electron density around the carbonyl oxygen [5], diminishing the double bond character of the carbonyl group, and shifting the stretching band to lower frequencies. The band at 1666 cm^{-1} is attributed to the C=O stretching of the amides not involved in hydrogen bonding, while the band at 1648 cm^{-1} is attributed to the amides participating in hydrogen bonding. As the number of side chains in the polymer increases, the band at 1648 cm^{-1} becomes more intense compared to the other band, demonstrating an increase in hydrogen bonding in the copolymers.

Also, the presence of the nitro group in the copolymers is observed in

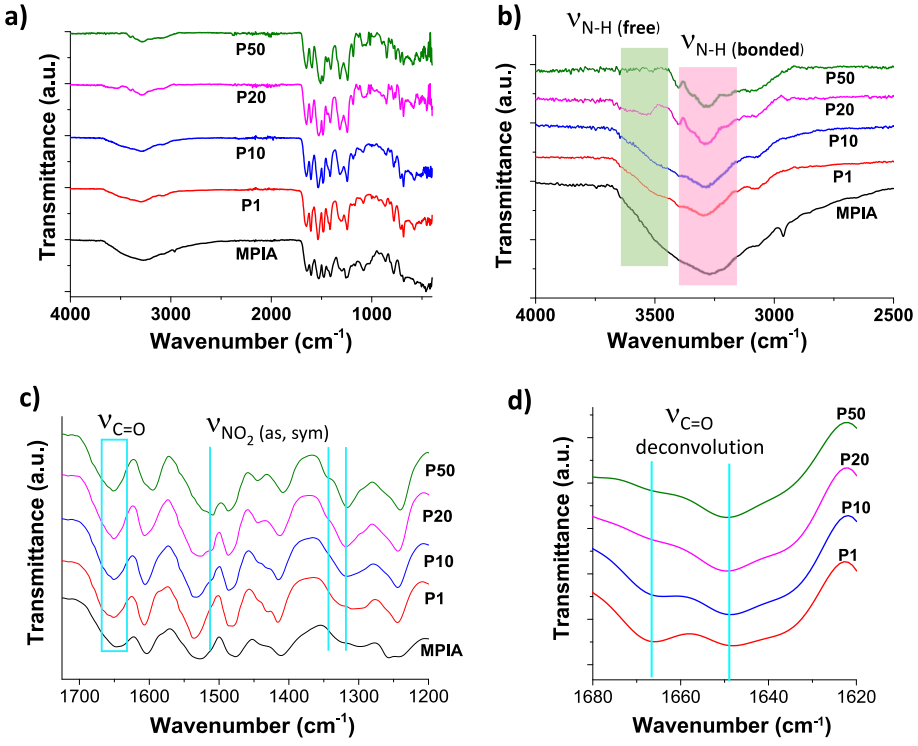

Figure 3. Comparative FTIR spectra of **P1**, **P10**, **P20**, **P50** and **MPIA**. a) Full spectrum, b) expansion between 4000 and 2500 cm^{-1}, c) spectrum expansion between 1700 and 1200 cm^{-1}, and d) deconvolution of the C=O stretching band of **P1**, **P10**, **P20** and **P50** .

the FTIR spectrum, becoming visible as the number of side chains increases. -NO_2 asymmetric stretching band is observed at 1508 cm^{-1} while two bands are observed for -NO_2 symmetric stretching at 1316 and 1345 cm^{-1}, as pointed out in blue in Figure 3c).

3.2.3. Thermal properties of the aromatic copolyamides

The thermal behaviour of the copolymers was characterized using TGA and DSC to evaluate both the thermal degradation and the thermal transitions and to compare them with **MPIA**. The thermal degradation of the polymers was assessed in terms of T_5, T_{10} and LOI (Table 2). The decrease in both T_5 and T_{10} temperatures of the new copolymers compared to **MPIA** (reference material) can be attributed to the presence of side chains. The side chains present in the copolymers are relatively short compared to the polymer main chain. When these short side chains break down under heat, they form smaller, more volatile fragments that can escape more easily compared to the breakdown of the main polymer chain. This results in a more pronounced decrease in T_5 and T_{10} values due to the volatile low mass fragments, particularly evident with a higher number of side chains, both under air and nitrogen atmospheres. Regarding char yield under nitrogen atmosphere, two simultaneous effects must be considered. The presence of *p*-aramid side chains increases hydrogen bonding, enhancing char yield compared to MPIA. However, the short side chains break down and evaporate first due to their lower molecular weight, reducing char yield value, which is only noticeable as side chains percentage increases. Thus, **P1** and **P10** have higher char yield than **MPIA**, but further increasing side chain percentage lowers the char yield due to side chain breakdown upon heating. Consequently, the Limiting Oxygen Index (LOI) value increases for **P1** and **P10** compared to **MPIA**, indicating improved resistance to combustion in these copolymers.

The T_g of the copolymers was also determined and compared to the T_g of the prepared **MPIA** (Figure 4a) and Table 2). The T_g was almost the same for **P1** and **MPIA**, showing no influence of the side chain in this thermal transition with minimal modification of the chemical structure. However, **P10** with 10% side chains shows a decrease in the T_g value since the bulky side chains prevent hydrogen interchain interactions from being established among the aramid backbones. On the other hand, when the percentage of *p*-amide containing side chains increases in the aramid, the T_g increases considerably. This can be attributed to the fact that with higher *p*-amide side chain content, the hydrogen bond interactions among the side chains prevail over the effect of its bulkiness. Also, it can be related to the lower polymer mobility of the chains due to the number of bulky side groups. Figure 4b) illustrates the evolution of the T_g of the copolymers as a function of the percentage of *p*-aramid side chains, highlighting the dual effects of the side chain bulkiness and hydrogen bond interactions.

3.2.4. Wide angle powder X-ray scattering

The X-ray diffraction pattern of reference *m*-aramid and copolymers **P1**, **P10**, and **P20** was acquired using unoriented polymer films (Figure 5). Commercial *m*-aramid film showed an amorphous diffraction pattern (broad halo) while **P1**, **P10** and **P20** displayed an amorphous pattern with some crystalline domains (narrow diffraction peaks), especially in copolymer **P1**. This observation suggests that copolymer **P1** exhibits heightened intermolecular interactions compared to **P10** and **P20**. While one might anticipate **P10** and **P20** to showcase a greater presence of crystalline domains due to the abundance of amide groups in their side chains, capable of interacting with amides in neighboring chains, it is noteworthy that **P1** displayed a higher occurrence of crystalline domains. This discrepancy could be attributed to increased chain mobility in **P1**, allowing the polymer chains to orient during film formation. This fact is influenced by the film preparation process (casting), during which the polymer chains have varying degrees of mobility, directly related to the intrinsic viscosity observed for each copolymer (Table 1). The intrinsic viscosity of the copolymers increased in the order of **P1**, **P20**, and **P10**. The lower viscosity of **P1** likely allows the copolymer side chains to reorient more readily during casting procedure, leading to a higher degree of crystallinity observed in the X-ray diffraction pattern compared to **P10** and **P20**. For the same reason, **P20** with a lower intrinsic viscosity than **P10** shows a higher presence of crystalline domains than **P10**. Using the 2θ value from XRD analysis, we calculated the interchain distance of the polymers using the equation $<R> = 5/8(\lambda/\sin\theta_{max})$. We observed that the interchain distance decreases from **MPIA** (4.74 Å) to **P20** (4.67 Å) as the percentage of side chains increases. This indicates that in the solid state, the side chains are oriented to maximize interactions between the polymer chains, such as hydrogen bonding and π-π stacking, thereby slightly reducing the distance between them.

Table 2
Thermal TGA data of the films under nitrogen atmosphere and synthetic air.

Polymer	Tg	Nitrogen atmosphere			Synthetic air atmosphere			LOI[c]
		T_5^a(°C)	T_{10}^b (°C)	Char yield (%)	T_5^a (°C)	T_{10}^b (°C)	Char yield (%)	
P1	273	399	450	62	419	461	1	43
P10	238	398	448	59	412	456	0	41
P20	269	397	443	52	389	430	4	38
P50	316	356	403	48	371	406	0	37
MPIA[d]	277	448	461	51	448	464	1	38

[a]5% weight loss temperature (T_5), 10% weight loss temperature (T_{10}); [b] at 800 °C; [c] limiting oxygen index, calculated from the TGA data [9] (LOI = 17.5 + 0.4 CR, where CR is the char yield in % weight at 800 °C). [d] MPIA synthesized in the laboratory.

3.2.5. Mechanical properties of the copolyamides

The mechanical performance of the aramids was evaluated using films derived from these materials. Unfortunately, the mechanical properties of **P50** could not be measured due to its significant insolubility at concentrations higher than 4% (mass/volume), preventing the preparation of films. Notably, the Young's Modulus of the prepared aramids shows significant improvement compared to **MPIA**, as depicted in Figure 6 (and in Figure S13 in SI, Section S3, showcasing stress-strain curves). Incorporating just 1% *p*-aramid side chains leads to a 48% increase in Young's modulus relative to **MPIA**. This enhancement slightly diminishes with increasing amounts of *p*-aramid chains present in the *m*-aramid, but the difference is not significant. These minimum differences can be related to the presence of more crystalline domains in **P1** compared to **P10** and **P20**. Higher crystallinity enhances stiffness by providing a more ordered molecular structure that resists deformation, exhibiting greater modulus due to well-defined crystalline domains that reinforce the material. As mentioned earlier, the crystallinity of these aramids is influenced by both the bulkiness of the side groups and the chain mobility of the copolymers, which in turn affects the interactions between side chains and the overall stiffness of the material. These findings underscore the effect of side chain proportion on the mechanical properties of *m*-aramids. As expected, elongation at break in the new copolymers remain lower than for **MPIA**, as a result of the increase in the Young's modulus. It is important to note that the relationship between crystallinity, Young's modulus, and tensile strength and elongation at break is not linear and depend on other factors such as the molecular structure and the material's processing.

Although no significant differences were observed in the Young's Modulus among the different copolymers that would justify the preparation of copolymers with a higher percentage of *p*-aramid side chain than for **P1**, the introduction of 20% *p*-aramid side chains in **P20** additionally results in an improvement of the tensile strength compared to **MPIA**. Although the evaluation of the properties of the copolymers showed that **P1** is a copolymer with better heat resistance and Young's modulus than **P20**, the evaluation of **P20**'s mechanical performance has highlighted that incorporating *p*-aramid side chains into *m*-aramids

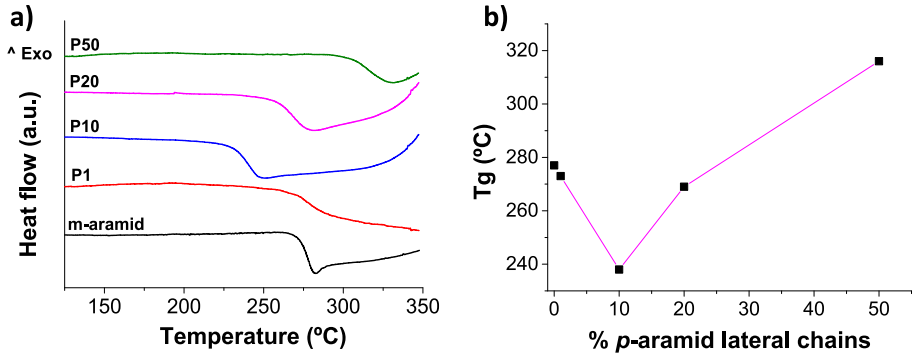

Figure 4. Thermal transitions of the synthesized polymers. a) DSC thermograms, and b) T_g of the polymers as a function of the percentage of *p*-aramid side chains

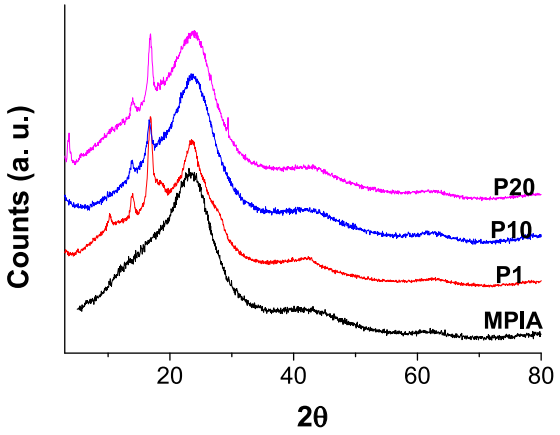

Figure 5. X-ray scattering of polymers **P1**, **P10**, **P20** and reference **MPIA**.

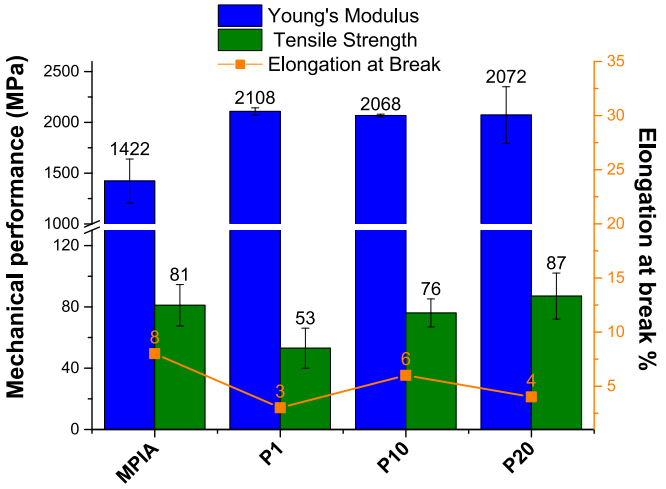

Figure 6. Mechanical performance of **P1**, **P10**, **P20** and **P50**, and comparison with **MPIA**.

leads to materials that exhibit increased stiffness, rigidity, and tensile strength compared to **MPIA,** which might be preferable compared to **P1** for some applications. Accordingly, we have performed a proof of concept with **P20** copolymer. This comprehensive enhancement underscores the effectiveness of this design strategy in optimizing the mechanical properties of *m*-aramids for diverse applications.

4. Proof of concept for a potential application

In the pursuit of cleaner energy solutions, hydrogen is emerging as a promising alternative. However, the storage of hydrogen presents unique challenges, particularly related to the embrittlement of steel used in high-pressure storage tanks. Exposure to hydrogen can induce embrittlement, reducing the operational lifespan of storage tanks and posing safety risks. To address these challenges, specialized polymer coatings offer a viable solution by serving as effective barriers against hydrogen permeation. By applying polymer coatings onto steel surfaces used for hydrogen storage, researchers aim to enhance durability and safety, thus advancing the feasibility and reliability of hydrogen storage systems.

In this sense, after demonstrating the enhanced properties of the synthesized copolymers compared to **MPIA**, we conducted a proof-of-concept study using **P20** in a hydrogen atmosphere to simulate its potential application as a polymer coating on steel or in another application in which a polymer enters into contact with hydrogen such as components for fuel cells and electrolyzers.

Accordingly, **P20** copolymer, having remarkable stiffness, rigidity, and tensile strength, is a prospective material that can be used as steal coating. Moreover, the terminal nitro groups in the copolymer have the ability to be reduced to amino groups in the presence of hydrogen, as observed during the monomer synthesis (Figure 7).

The proof-of-concept experiment involved placing a **P20** film inside a hydrogenation vessel overnight, under a hydrogen pressure of 70 psi. In a typical reduction reaction of nitro to amino groups with hydrogen, a Pd/C catalyst is often used to ensure full conversion in short periods of time. Therefore, we also prepared another film incorporating 2% weight of Pd/C catalyst along with **P20** using the solution casting method, and subjected it to the same hydrogenation conditions for comparison, to be able to attribute the possible changes in the mechanical performance to the presence of amino groups in the copolymer instead of nitro groups. The films were evaluated for changes in the Young's modulus and thermal performance after exposure to the hydrogen atmosphere. The experimental results are presented in Figure 8, illustrating the effects of hydrogen exposure on the properties of the **P20** polymer films. This time, the Young's modulus of all the films was measured using AFM (Atomic Force Microscopy) because the catalysts caused the material to become too brittle to be measured using a universal testing machine, and an MPIA film was used as a control experiment.

As observed, **P20** films exhibited enhanced performance after exposure to hydrogen, attributed to the reduction of nitro functional groups in the polymer to amine groups and the formation of additional hydrogen bonds with side groups. The film prepared with the catalyst showed a lower Young's modulus due to the embrittling effect of carbon particulates from the catalyst. However, when subjected to a hydrogen atmosphere, the Young's modulus improved to a greater extent compared to films without the catalyst. This improvement suggests a higher conversion of nitro groups to amino groups facilitated by the

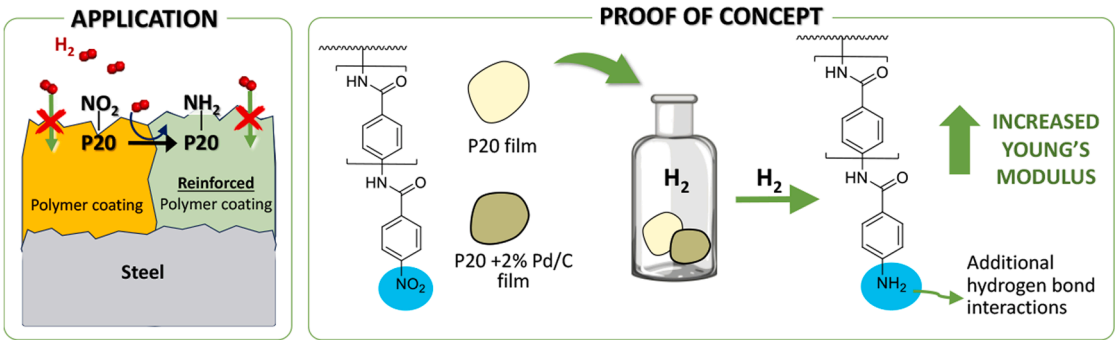

Figure 7. Possible application and proof of concept with **P20**.

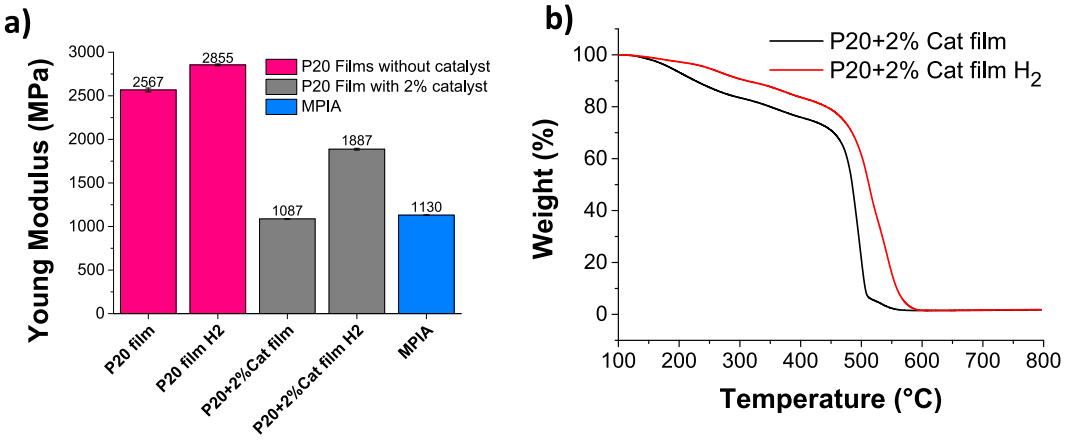

Figure 8. Properties of **P20** films before and after contact with H_2. MPIA film was used as control experiment. a) Young's modulus (Young's moduli in this proof-of-concept were measured using AFM instead of tensile tests; therefore, the values are not comparable with those depicted in Figure 6), and b) Thermogravimetric analysis.

catalytic effect of Pd/C, resulting in increased hydrogen bond formation through the amino groups. Such polymers hold potential as hydrogen permeation barrier coatings for high-pressure hydrogen storage vessels, offering a cost-effective solution to mitigate hydrogen embrittlement and support the growth of the hydrogen industry. The most recent studies on polymeric steel coatings designed for hydrogen storage and/or transport suggest that crystalline polymers with high Young's moduli are the most effective for these purposes [15]. Therefore, we believe that using materials that increase their Young's modulus in the presence of hydrogen could be very beneficial for this industry.

The improvement of the thermal performance of the polymer after being exposed to hydrogen was demonstrated in the TGA thermogram of the films containing the catalyst as well, which also proves the additional hydrogen bond formation. Nonetheless, for actual applications such as steel coating, no catalyst would be used in the polymer formulation, as its presence adversely affects the mechanical performance of the film.

This way, the polymer not only protects steel from hydrogen, but also in contact with hydrogen, the coating becomes more efficient in terms of mechanical and thermal performance to act as a barrier.

5. Conclusions

In summary, this study outlines a novel approach to enhance the mechanical performance of high-performance aromatic polyamides, commonly known as aramids. The strategy involves incorporating *p*-aramid side chains into *m*-oriented aramids through copolymerization. The resulting copolymers demonstrated significant improvements in both Young's modulus and tensile strength compared to the commercial *m*-aramid, MPIA. Additionally, the introduction of a nitro group to cap the *p*-aramid side chains proved highly effective in augmenting mechanical performance in environments with hydrogen exposure. These findings suggest promising applications for protective coatings in high-pressure hydrogen storage environments, specifically to mitigate embrittlement and improve operational lifespan of steel storage systems.

Funding

This work was supported by the Regional Government of Castilla y León (Junta de Castilla y León), the Ministry of Science and Innovation MICIN and the European Union NextGenerationEU/PRTR, and the Spanish Agencia Estatal de Investigación (State Research Agency). Author M. Trigo-López received grant PID2019-108583RJ-I00 funded by MCIN/AEI/ 10.13039/501100011033. Álvaro Miguel-Ortega received funding from Ministerio de Universidades-European Union in the frame of NextGenerationEU RD 289/2021 (CA1/RSUE/2021-00409) by the Universidad Autónoma de Madrid.

CRediT authorship contribution statement

Álvaro Miguel Ortega: Validation, Investigation, Formal analysis, Data curation. **Sául Vallejos:** Validation, Methodology, Funding acquisition. **José Miguel García:** Writing – original draft, Validation, Formal analysis. **Miriam Trigo-López:** Writing – original draft, Visualization, Validation, Investigation, Funding acquisition, Conceptualization.

Declaration of competing interest

The authors declare that they have no known competing financial

interests or personal relationships that could have appeared to influence the work reported in this paper.

Data availability

The raw or processed data necessary to replicate these results are available at https://riubu.ubu.es/handle/10259/5684 under the name "UBU-Polymers Research Group 21082024".

Acknowledgements

The authors acknowledge with gratitude the financial support received from all funding sources.

Appendix A. Supplementary data

Supplementary data to this article can be found online at https://doi.org/10.1016/j.eurpolymj.2024.113397.

References

[1] K. Marchildon, Polyamides – still strong after seventy years, Macromol. React. Eng. 5 (2011) 22–54, https://doi.org/10.1002/mren.201000017.
[2] M. Trigo-López, J.M. García, J.A.R. Ruiz, F.C. García, R. Ferrer, in: Aromatic Polyamides, John Wiley & Sons Inc, Hoboken, NJ, USA, 2018, pp. 1–51, https://doi.org/10.1002/0471440264.pst249.pub2.
[3] J.M. García, F.C. García, F. Serna, J.L. de la Peña, High-performance aromatic polyamides, Prog. Polym. Sci. 35 (2010) 623–686, https://doi.org/10.1016/j.progpolymsci.2009.09.002.
[4] C.L. Lewis, K. Stewart, M. Anthamatten, The Influence of hydrogen bonding side-groups on viscoelastic behavior of linear and network polymers, Macromolecules. 47 (2014) 729–740, https://doi.org/10.1021/ma402368s.
[5] C. Yang, H. Wu, Y. Dai, S. Tang, L. Luo, X. Liu, Self-enhancement in aramid fiber by filling free hydrogen bonding interaction sites in macromolecular chains with its oligomer, Polymer (Guildf). 180 (2019) 121687, https://doi.org/10.1016/j.polymer.2019.121687.
[6] Y. Ohta, T. Shirakura, A. Yokoyama, T. Yokozawa, Synthesis of polystyrene- graft -poly(p -benzamide) by chain-growth condensation polymerization and radical polymerization: improvement of thermal properties of polystyrene, J. Polym. Sci. Part A Polym. Chem. 51 (2013) 1887–1892, https://doi.org/10.1002/pola.26548.
[7] P. Kong, S. Drechsler, S. Balog, S. Schrettl, C. Weder, A.F.M. Kilbinger, Synthesis and properties of poly(norbornene)s with lateral aramid groups, Polym. Chem. 10 (2019) 2057–2063, https://doi.org/10.1039/C9PY00187E.
[8] C.J. Reese, Y. Qi, D.T. Abele, M.D. Shlafstein, R.J. Dickhudt, X. Guan, M.J. Wagner, X. Liu, S.G. Boyes, Aromatic Polyamide brushes for high young's modulus surfaces by surface-initiated chain-growth condensation polymerization, Macromolecules. 55 (2022) 2051–2066, https://doi.org/10.1021/acs.macromol.1c02088.
[9] D.W. van Krevelen, K. te Nijenhuis, Properties of Polymers. Their Correlation with Chemical Structure; Their Numerical Estimation and Prediction from Additive Group Contributions, 4th ed.,, Elsevier, Amsterdam, 2009.
[10] D. Harwood, H. Aoki, Y.-D. Lee, J.F. Fellers, J.L. White, Solution and rheological properties of poly(m-phenyleneisophthalamide) in dimethylacetamide/LiCl, J. Appl. Polym. Sci. 23 (1979) 2155–2168, https://doi.org/10.1002/app.1979.070230726.
[11] S. Benaglia, C.A. Amo, R. Garcia, Fast, quantitative and high resolution mapping of viscoelastic properties with bimodal AFM, Nanoscale. 11 (2019) 15289–15297, https://doi.org/10.1039/C9NR04396A.
[12] M. Trigo-López S. Vallejos J.A. Reglero Ruiz A. García-Gómez M. Seara-Martínez F. C. García J.M. García High-performance nanoporous aramid films reinforced with functionalized carbon nanocharges using ionic liquids Polymer (Guildf). 202 (2020) 122629 10.1016/j.polymer.2020.122629.
[13] M. Trigo-López, J.L. Barrio-Manso, F. Serna, F.C. García, J.M. García, Crosslinked aromatic polyamides: a further step in high-performance materials, Macromol. Chem. Phys. 214 (2013) 2223–2231, https://doi.org/10.1002/macp.201300342.
[14] K. Li, L. Luo, J. Huang, X. Ma, H. Wang, Y. Feng, X. Liu, The evolution of structure and properties for copolyamide fibers–containing benzimidazole units during the decomplexation of hydrogen chloride, High Perform. Polym. 28 (2016) 381–389, https://doi.org/10.1177/0954008315583704.
[15] Y. Lei, E. Hosseini, L. Liu, C.A. Scholes, S.E. Kentish, Internal polymeric coating materials for preventing pipeline hydrogen embrittlement and a theoretical model of hydrogen diffusion through coated steel, Int. J. Hydrogen Energy. 47 (2022) 31409–31419, https://doi.org/10.1016/j.ijhydene.2022.07.034.